*Korean J. Chem. Eng.*, 37(8), 1419-1426 (2020)
DOI: 10.1007/s11814-020-0576-4

pISSN: 0256-1115
eISSN: 1975-7220

# Colloidal synthetic methods of amorphous molybdenum phosphide nanoparticles for hydrogen evolution reaction catalysts

**Hyeri Kang*,‡, Taegyeom Lee*,‡, Yoonsu Park*, Yun-Kun Hong*, Miri Choi**, Jiung Cho***, and Don-Hyung Ha*,†**

*School of Integrative Engineering, Chung-Ang University, Seoul 06974, Korea
**Chuncheon Center, Korea Basic Science Institute, Chuncheon 24341, Korea
***Western Seoul Center, Korea Basic Science Institute, Seoul 03579, Korea
(*Received 31 March 2020 • Revised 10 May 2020 • Accepted 11 May 2020*)

**Abstract**−Transition metal phosphides (TMPs) have recently emerged as promising hydrogen evolution reaction (HER) catalytic alternatives to platinum. Among them, molybdenum phosphide (MoP) has attracted extensive attention due to its high electrical conductivity, good stability, and Pt-like electronic structure; however, there is no systematic comparison of its different colloidal synthetic routes. This study systematically compares two colloidal synthetic methods, one-pot and two-step, for amorphous MoP and the associated morphological changes during their reaction time. The amorphous MoP nanoparticles synthesized via the two-step method within 4 h exhibited the highest HER performance with an overpotential of 177 mV in 0.50 M $H_2SO_4$ for a current density of −10 mA $cm^{-2}$; this might be due to their highly developed Mo-P bondings revealed by X-ray photoelectron spectroscopy analysis. Thus, this work demonstrates that the HER catalytic performance of MoP can be significantly influenced by its synthetic method and reaction time.

Keywords: Hydrogen Evolution Reaction, Transition Metal Phosphide, Molybdenum Phosphide Nanoparticle, Colloidal Nanoparticle, Electrocatalyst

## INTRODUCTION

Hydrogen is an ideal energy carrier alternative to fossil fuels due to its large energy density, renewability, and environmentally friendly nature [1,2]. Among its many production methods, electrolysis has been extensively studied because it provides high-purity products and prevents $CO_2$, unlike conventional hydrogen gas generation techniques such as steam reforming, biomass pyrolysis, and coal gasification [3,4]. The efficiency of hydrogen production through water electrolysis highly relies on the catalyst performance; thus, high-performance catalysts allowing the relatively low-cost commercialization of an electrolyzer generating H are crucial [5-7].

Pt-based catalysts show the highest hydrogen evolution reaction (HER) performance and stability, but their practical applications are limited by their high cost and scarcity. To overcome such drawbacks, non-precious metal-based alternatives with high catalytic activity must be developed [8-10].

Studies on low-cost, earth-abundant, and highly active catalysts have proposed several material groups, including transition-metal carbides [11,12], transition-metal phosphides (TMPs) [13-15], transition-metal dichalcogenides [16,17] and transition-metal sulfides [18,19]. In particular, TMPs have emerged as promising HER catalysts due to their abundant sources, stability in a wide pH range, low cost, good conductivity, and high activity [20-24]. Various compositions and phases of several TMPs, such as CoP [22,25], $Co_2P$ [26], FeP [10,27,28], $Fe_2P$ [28], $Ni_2P$ [29,30], WP [31], and MoP [32,33], have been deeply investigated; among these TMPs, molybdenum phosphide has drawn much attention because of its good stability, high electrical conductivity, and Pt-like electronic structure [34,35].

Mo-based catalysts can adopt various structures and compositions, including MoB [36,37], MoN [12], $Mo_2C$ [12,36], $MoO_2$ [38], and $MoS_2$ [39,40]. They all present HER catalytic activity and MoP is one of the most active ones [33]. However, the synthetic methods for MoP nanomaterials are not well-established yet; in particular, the synthesis of colloidal MoP nanoparticles (NPs) has not been developed even though colloidal NPs are generally an ideal catalyst form to fabricate electrodes.

Many different nanocatalyst fabrication techniques, such as chemical vapor deposition [41,42], atomic layer deposition [43,44], pyrolysis [45,46], electrochemical method [47-49], and colloidal method, have been studied. Among them, the colloidal synthetic method provides a high dispersion in organic solvents and monodispersity. Moreover, various NP compositions and morphologies can be controlled in a colloidal synthesis by adjusting the precursors and reaction conditions [50-53].

There are two typical approaches to synthesize colloidal metal phosphide NPs: the one-pot [54-57] and the two-step method [10,22,58]. In the one-pot technique, all the precursors, the solvent, and the surfactant ligands are added at the beginning of the reaction. This method has relatively high yield, simplified processing, and is time-saving compared to the two-step approach. In the two-step method, instead, the metal NPs are first synthesized and then in-

†To whom correspondence should be addressed.
E-mail: dhha@cau.ac.kr
‡These authors contributed equally.

jected into an activated phosphorus source solution to obtain metal phosphide NPs; compared to the one-pot method, it has the advantage of providing sophisticated size distribution. However, these two methods and the respective changes in the amorphous MoP during their reaction time have not been systematically compared yet.

In this work, the catalytic activity and morphological changes between these two methods were compared at controlled reaction times. Despite the fact that all the NP samples exhibited similar size and shape, diverse catalytic performance was observed according to the synthetic approach and the reaction time; in particular, the NPs synthesized via the two-step method showed high HER catalytic activity, which was attributed to their more abundant Mo-P bonding. The results of this study demonstrate that the synthetic method and the reaction time can significantly influence the HER performance of MoP catalysts.

## EXPERIMENTAL SECTION

### 1. Chemicals

Molybdenum hexacarbonyl ($Mo(CO)_6$, 98%), trioctylphosphine (TOP, 97%), 1-octadecene (ODE, 90%, technical grade), and oleylamine (OLA, 70%, technical grade) were purchased from Sigma-Aldrich. Squalane (98%) was obtained from Alfa-Aesar. Sulfuric acid ($H_2SO_4$; 1.0 N) was provided by Thermo Fisher Scientific. All the chemicals were used without further purification.

### 2. MoP NP Synthesis via the Two-step Method

2-1. Synthesis of Mo NPs

Molybdenum NPs were first synthesized to perform their phase transformation into MoP NPs. ODE (30.8 mL) and OLA (0.62 mL) were added to a 50 mL three-necked flask equipped with an evaporator trap, a thermometer, a thermometer adapter, a rubber septum, and a magnetic stir bar. To remove water molecules and volatile chemicals, the ODE/OLA solution was heated to 120 °C and maintained for 1 h at this temperature under vacuum; next, this solution was placed under nitrogen gas condition and $Mo(CO)_6$ (4 mmol) was added, followed by heating to 230 °C and maintaining this temperature for 30 min.

2-2. Synthesis of MoP NPs

To convert the Mo NPs into MoP NPs, TOP (6 mL) and squalene (14 mL) were added to a separate 50 mL three-necked flask. This solution was degassed at 120 °C for 1 h to eliminate impurities and then heated and maintained at 350 °C for 1 h to activate TOP; under this condition, the solution became yellowish green. After the activation process, the solution temperature was lowered to 320 °C and the Mo NP solution (10 mL) was added to it. The resulting mixture was kept at 320 °C for different phosphorization reaction times (30 min, 2 h, and 4 h). All the samples were washed with acetone/hexane and centrifuged for 5 min at 7,000 rpm; this washing process was repeated three times. Then, the purified NPs were stored in hexane.

### 3. MoP NP Synthesis via the One-pot Method

Squalane (21 mL, 40.23 mmol) and TOP (3 mL, 20.19 mmol) were added to a 50 mL three-necked flask. To remove water molecules and volatile chemicals, this solution was heated to 120 °C and maintained for 1 h at this temperature under vacuum. Then, the flask was placed under nitrogen gas environment and $Mo(CO)_6$ (792 mg, 3 mmol) was added. This reaction mixture was heated to 320 °C and maintained there for different reaction times (30 min, 2 h, and 4 h); the solutions became yellowish after reaching 200 °C and turned black at 320 °C. Next, all the samples were washed with acetone/hexane and centrifuged for 5 min at 7,000 rpm. This cleaning process was repeated three times. Finally, the purified NPs were stored in hexane.

### 4. Material Characterization

X-ray diffraction (XRD) analysis was performed by using an AXS New D8 ADVANCE diffractometer (Bruker) with a Cu K$\alpha$ radiation source and a LynxEye line detector; for this analysis, the MoP NP ink (NPs dispersed in hexane) was drop-cast on a zero-background quartz support. Transmission electron microscopy (TEM) images were acquired with a JEM-2100 microscope (JEOL) at an accelerating voltage of 200 kV. High-resolution TEM (HRTEM) images were collected by using a JEM-2100F (JEOL) at 200 kV. X-ray photoelectron spectroscopy (XPS) analysis involved using a K-alpha+ spectrometer (Thermo Fisher Scientific) using an Al K$\alpha$ radiation source. Energy-dispersive spectroscopy (EDS) analysis was acquired using a Carl Zeiss SIGMA microscope. The EDS results are the averaged measurement value of the three parts.

### 5. Electrochemical Measurements

The HER activity of the MoP NPs synthesized with the two synthetic methods and different reaction times was assessed through electrochemical measurements. The working electrode was fabricated by dispersing the MoP NPs in hexane at a concentration of 8 mg $mL^{-1}$ and drop-casting the as-obtained MoP NP ink (5 μL) onto 0.25 $cm^2$ Ti foils, followed by annealing for 2 h at 450 °C under $H_2$ (5%)/Ar (95%) gas flow to remove the surfactants from the MoP NP surfaces. The electrochemical measurements were carried out in a 0.5 M $H_2SO_4$ solution by using a standard three-electrode cell consisting of a saturated calomel electrode (SCE) as the reference electrode, a graphite rod as the counter electrode, and the various MoP NP samples as the working electrode. Linear sweep voltammetry (LSV) analysis of HER was performed in a 0.5 M $H_2SO_4$ solution at a scan rate of 5 mV $s^{-1}$ within a potential range between −0.25 and −0.7 V (vs. SCE). To measure the internal resistance of the electrochemical cell, electrochemical impedance spectroscopy (EIS) measurements were conducted at frequencies ranging from 100 kHz to 0.1 Hz at −0.35 V (vs. SCE) by using an alternating current signal amplitude of 10 mV. The double-layer capacitance ($C_{dl}$) was evaluated via cyclic voltammetry (CV) in the potential of the non-Faradaic region from −0.25 to 0.05 V (vs. SCE) at different scan rates (20, 40, 60, 80, and 100 mV $s^{-1}$) to determine the catalytic active surface area of the samples. Linear slope fitting was done by plotting the charging current densities at –0.05 V (vs. SCE) for each scan rate. All the acquired data were iR-corrected for the solution resistance.

## RESULTS AND DISCUSSION

Scheme 1 illustrates the two methods adopted to synthesize colloidal MoP NPs. One method is a one-pot reaction that produces NPs by adding all the precursors, solvent, and surfactant ligands together in one vessel from the beginning of the reaction. The other is a two-step reaction in which metal NPs are first synthesized and

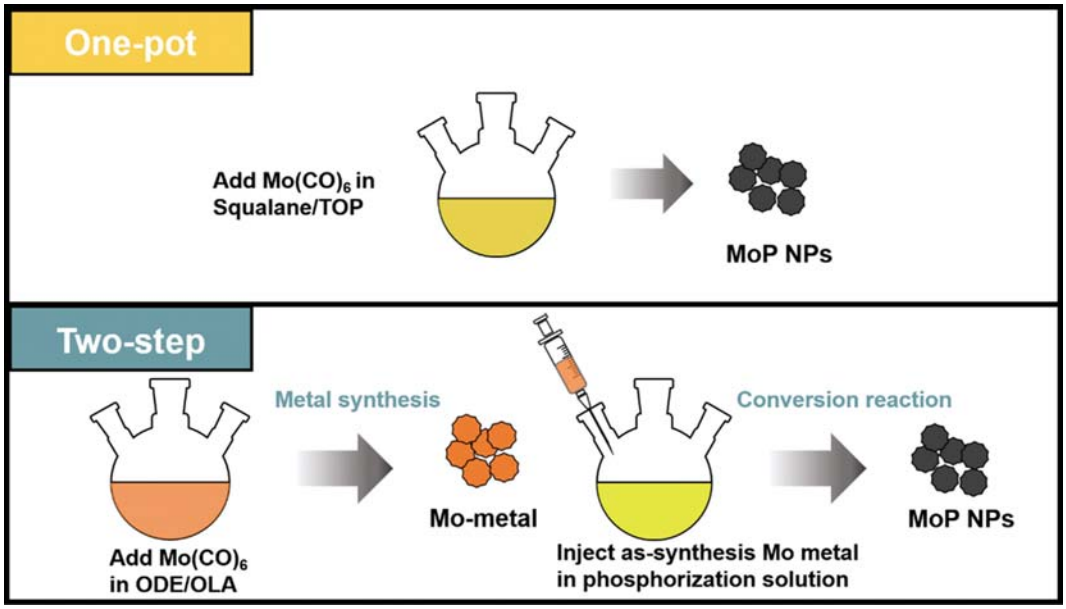


**Scheme 1. Colloidal synthesis of MoP nanoparticles (NPs) via the one-pot and the two-step method.**

then the Mo metal solution is injected into an activated phosphorus source solution to produce metal phosphide NPs through conversion reaction. Various phosphorus sources are commonly used for the phosphorization reaction from metal to metal phosphide, such as TOP [58], triphenylphosphite [59], tri-*n*-butylphosphine [60], tris(diethylamino)phosphine [61], and tris(dimethylamine)phosphine [62]. To examine the influence of the P source type on the MoP NP synthesis, all these sources were preliminarily tested, confirming the dependence of the electrocatalytic activity of the MoP NPs on this variable (Fig. S1). Since the MoP NPs prepared by using TOP exhibited the highest catalytic performance, successive experiments in this work were performed with TOP as the only P source.

The morphological differences among the MoP NPs synthesized via the two methods and various reaction times were compared by TEM observation (Fig. 1(a)-(g)). In the two-step method, after the injection of the Mo NPs solution, the size and shape of the NPs were maintained regardless of the reaction time thus, even after the phosphorization; this indicates that the nanoscale Kirkendall effect, typical in metal phosphide NPs, does not occur in this Mo-P system [25]. The NPs phosphorized with the two-step method for 30 min, 2 h, and 4 h were 4.08±0.54, 4±0.5, and 4.03±0.67 nm, respectively, presenting a similar size for all the reaction time. Their morphologies did not significantly differ from that of the starting Mo NPs (3.8±0.8 nm). The size and irregular shape of the MoP NPs did not change with the reaction time also in the case of the one-pot method. The one-pot synthesized MoP NPs showed 3.9±0.4, 3.9±0.4, and 3.9±0.6 nm after 30 min, 2 h, and 4 h, respectively, similarly to the sizes reported by previous studies on this synthetic route [33]. Thus, these TEM results indicate that the MoP NP growth does not directly depend on the synthetic method nor the reaction time.

The XRD analysis confirmed the MoP phase and the crystallinity of all the synthesized NPs, which were phosphorized at 320 °C (Fig. 1(h) and (i)). The one-pot synthesized MoP NPs exhibited a highly broad peak at ~40.9° independent of the reaction time, which

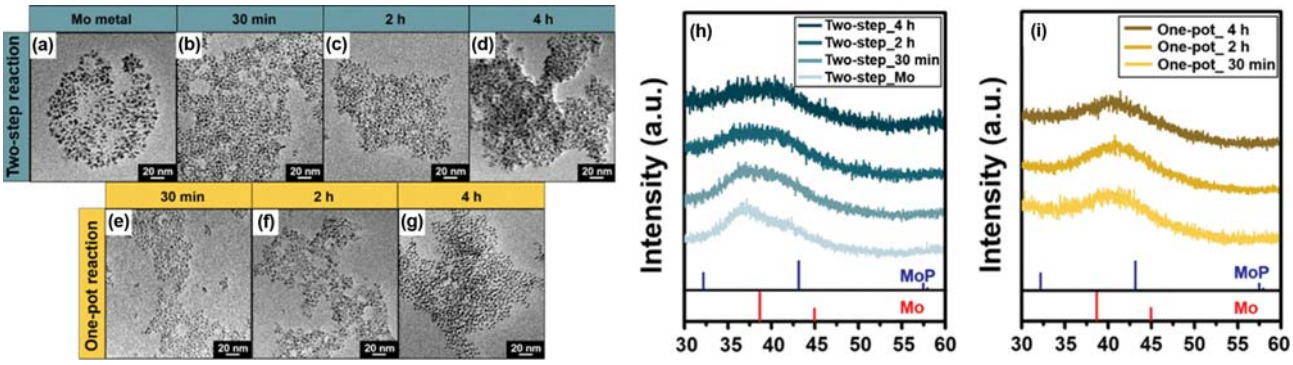


**Fig. 1. TEM images of Mo and MoP nanoparticles (NPs) synthesized via the (a)-(d) two-step and (e)-(g) the one-pot method MoP NPs with different reaction times. XRD patterns of the MoP NPs prepared through the (h) two-step and (i) the one-pot method; the red and blue bars correspond to the powder diffraction 01-089-2587 and 03-065-6024, respectively.**

is a typical XRD pattern for amorphous MoP NPs [33]. The pristine Mo metal sample showed one broad peak at ~37°, which is slightly shifted by 1.9° toward lower angles with respect to the main peak of the Mo reference; after the phosphorization by TOP, the XRD results revealed amorphous structures for all the reaction times, suggesting that the two-step method does not produce crystalline MoP NPs at least within the first 4 h of reaction. All the samples phosphorized within the two-step reaction presented a broad peak slightly shifted by 2.1° to lower angles with respect to that observed for the one-pot synthesized NPs. The general trend in the conversion reaction of phosphorization is as follows: the crystallinity increases along with the reaction time and highly activated phosphorus sources. However, the XRD patterns did not show this behavior for the two colloidal MoP synthetic methods investigated. Therefore, these XRD patterns demonstrate that crystalline MoP is not a favorable structure at a reaction temperature of 320 °C and for reaction times from 30 min to 4 h.

HR-TEM analysis was performed to confirm the crystallinity difference between the products of the two synthetics methods (Fig. 2(a)-(c)). The Mo NPs obtained in the first step of the two-step approach were irregularly shaped and semi-crystalline. The HR-TEM images of the MoP NPs produced via the two methods

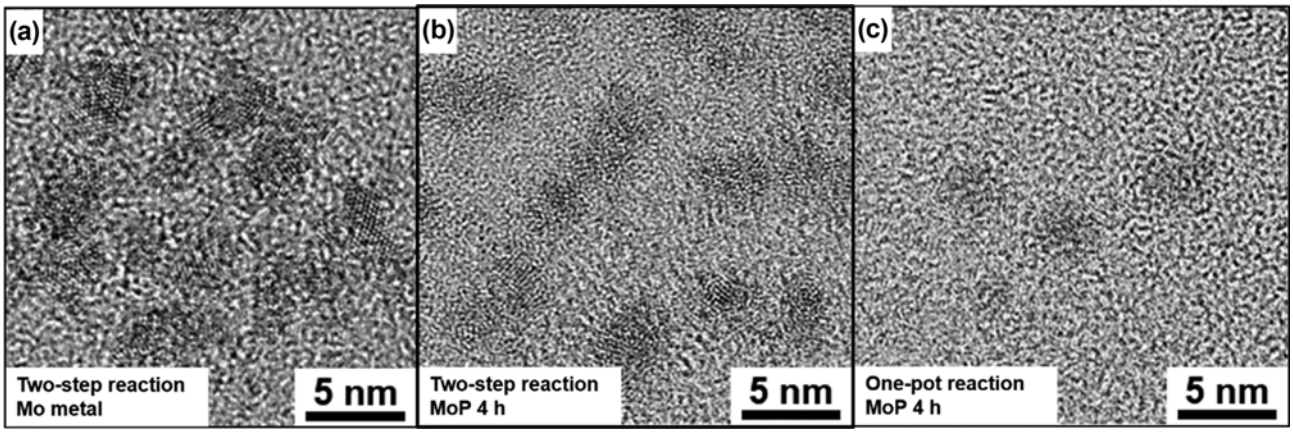


**Fig. 2. HR-TEM images of (a) Mo NPs and (b) MoP NPs of two-step reaction and (c) MoP NPs of one-pot reaction.**

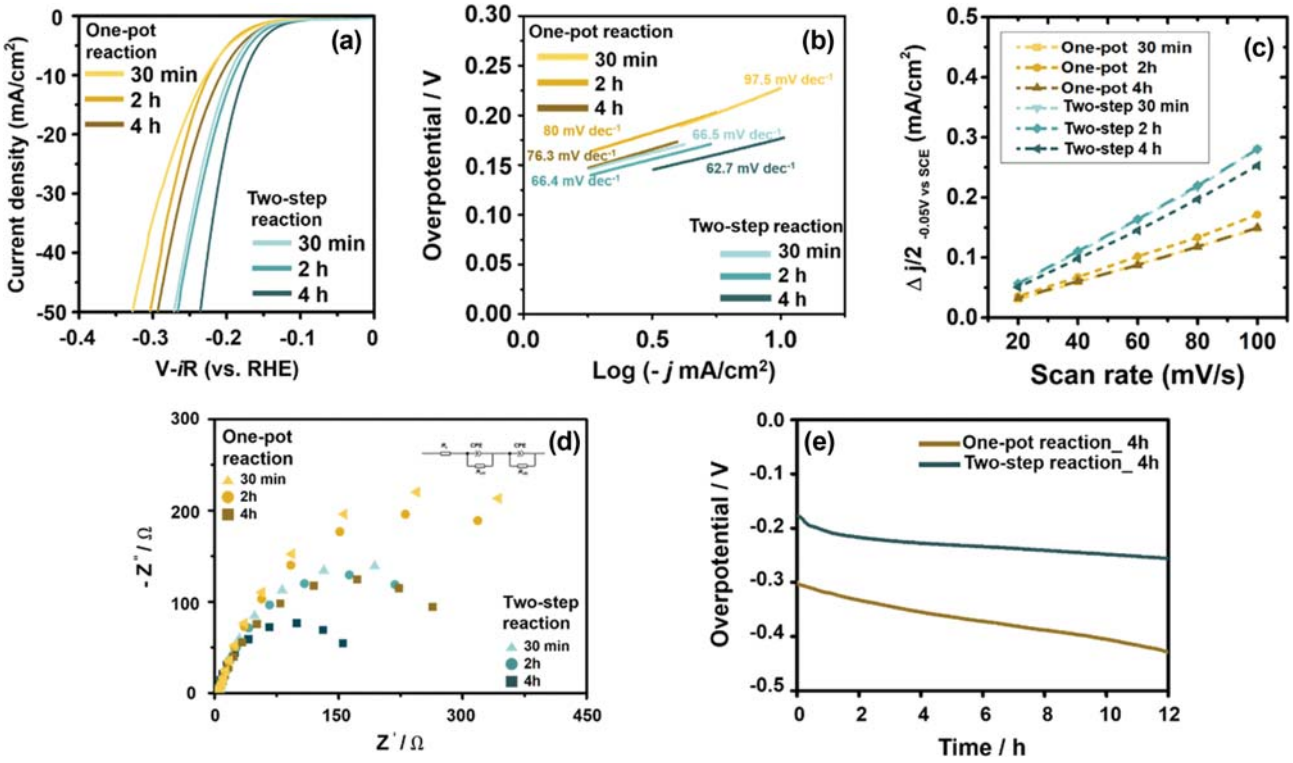


**Fig. 3. Electrocatalytic properties of the MoP nanoparticles (NPs) synthesized via the one-pot and the two-step method with different reaction times: (a) LSV curves, (b) corresponding Tafel polarization plots, (c) capacitive current densities as a function of the scan rate, (d) Nyquist plots (e) stability at a current density of 10 mA $cm^{-2}$.**

for a 4 h reaction time revealed amorphous structure, consistent with the XRD results. Hence, the HR-TEM observation further confirms that the synthetic method and the reaction time do not significantly influence the crystallinity of the MoP NPs.

To compare the electrocatalytic activities of the synthesized MoP NPs, catalyst films with a loading mass of 160 μg $cm^{-2}$ were prepared by drop-casting the NP ink on a Ti foil. The polarization curves for all the samples were acquired through iR-corrected LSV on the reversible hydrogen electrode. The electrocatalytic activity differed depending on the synthetic route and the reaction time; the LSV results showed higher catalytic activity, thus lower overpotential for longer reaction times for both methods (Fig. 3(a)). The overpotential of the one-pot synthesized MoP NPs reacted for 30 min, 2 h, and 4 h was 228, 224, and 208 mV, respectively, to achieve a current density of −10 mA $cm^{-2}$; in these conditions, the corresponding overpotential of the samples prepared via the two-step approach was 196, 190, and 177 mV, respectively. For the same reaction time, the activity of the MoP NPs fabricated through the two-step method was higher than that of that obtained via the one-pot technique. Thus, although the MoP NP morphology did not notably vary depending on the synthetic procedure, as shown in Fig. 1(a)-(f), the catalytic performance significantly changed according to the preparation conditions.

To further understand the HER catalytic mechanism of the MoP NPs, a Tafel analysis was performed by plotting overpotential versus current density of the log scale in the linear region of the electrochemical reaction. The Tafel slope for the HER can be 30, 40, and 120 mV $dec^{-1}$ corresponding to, respectively, the Tafel, Heyrovsky, and Volmer reactions [23]. The pathway forming hydrogen molecules on the catalyst surface through the HER mechanism is Volmer-Tafel or Volmer-Heyrovsky [23]. For the reaction time of 4 h, the Tafel slope of the MoP NPs prepared via the two-step method (62.7 mV $dec^{-1}$) was lower than that of the one-pot synthesized ones (76.3 mV $dec^{-1}$); this suggests that a higher HER rate can be obtained through the two-step approach (Fig. 3(b)). The low Tafel slope of the two-step synthesized MoP is comparable to that of other high-activity TMPs, such as FeP (64 mV $dec^{-1}$), CoP (60 mV $dec^{-1}$), and $Ni_{12}P_5$ (63 mV $dec^{-1}$). The Tafel slopes of the samples fabricated with the two-step method for 30 min, 2 h, and 4 h suggested the rate-determining step of Volmer-Heyrovsky by belonging to the Tafel slope of 62-67 mV $dec^{-1}$, implying that their HER catalytic mechanisms are similar to that of other highly active TMP catalysts [63,64].

The electrochemically active surface area (ECSA) of the samples was measured to fully understand their intrinsic activity (Fig. 3(c)). The $C_{dl}$ values, derived from the CV curves in the non-Faradaic current region (Fig. S2), of the MoP NPs synthesized via the one-pot method for 30 min, 2 h, and 4 h were, respectively, 1.47, 1.69, and 1.46 mF $cm^{-2}$, while those of the samples synthesized through the two-step approach were slightly higher. Although the MoP NPs prepared in the two ways for 4 h had a small active area, they both showed high activity with low overpotential, which implies a high intrinsic activity.

Nyquist plots fitted by a well-established equivalent circuit revealed the charge-transfer resistance ($R_{ct}$) related to the electrochemical activity of the synthesized catalysts for HER (Fig. 3(d)). Two $R_{ct}$ were observed ($R_{ct1}$ and $R_{ct2}$) as two semicircles at the same overpotential (−0.35 v SCE); $R_{ct1}$ can be considered the dominant factor between them since its value was 100 times larger than the $R_{ct2}$ one (Table S1). The $R_{ct1}$ value of the samples synthesized via the two-step method for 30 min, 2 h, and 4 h was 338, 319, and 181 Ω, respectively; these results well match the trend of the corresponding polarization curves, indicating higher activity from longer reaction times. For the reaction time of 4 h, the $R_{ct1}$ value for the sample prepared via the one-pot method (332 Ω) was almost two-times greater than that of the two-step synthesized one, demonstrating that the two-step method can enhance the charge transfer of electron on HER for the MoP NPs compared to the other approach.

A stability test was performed on the representative samples (two-step and one-pot for 4 h) for each synthetic method at 10 mA $cm^{-2}$ (Fig. 3(e)). The overpotential of the two-step synthesized MoP NPs increased from 177 to 256 mV after 12 h of long-term operation, while the durability of the samples prepared via the one-pot method for 4 h significantly dropped; thus, the two-step method is more suitable for long-term durability in acidic environments.

The atomic percent of the MoP NPs synthesized through the two methods was estimated via EDS (Fig. 4). The EDS results revealed a slight difference among the samples fabricated in the two ways with a reaction time: the one-pot reaction synthesized MoP NPs for all reaction time shared similar P/Mo ratios (1.21± 0.07), while the P/Mo ratios of sample prepared via the two-step method consistently increased from 0.87 to 1.54. This EDS result

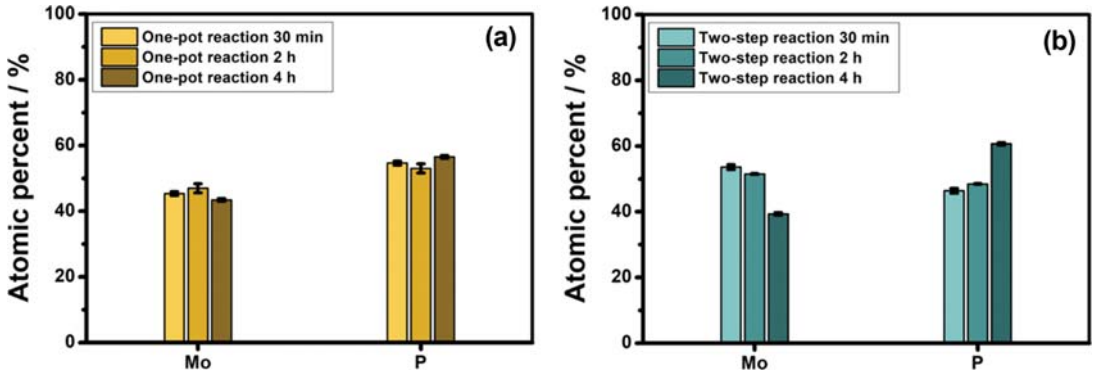


**Fig. 4. Energy dispersive spectroscopy results for MoP nanoparticles synthesized via (a) the one-pot and (b) the two-step method.**

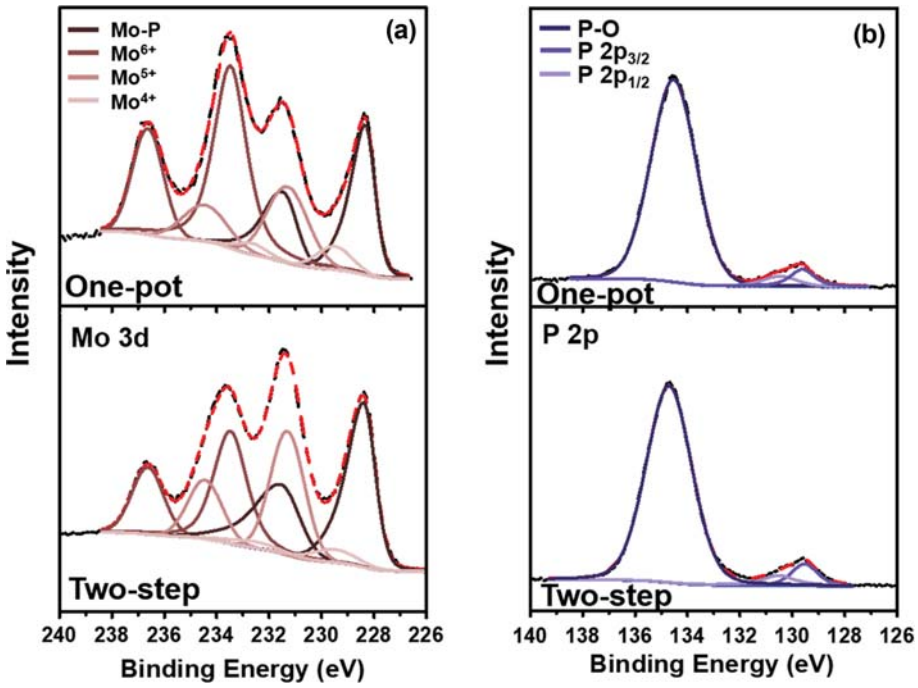


**Fig. 5. X-ray photoelectron (a) Mo 3d and (b) P 2p spectra of MoP nanoparticles synthesized via the two-step and the one-pot method.**

implied that the phosphorization mechanism differed according to synthetic methods. The P-rich TMP phase has been usually known to have higher catalytic HER activity than the metal-rich TMP phase [65,66]. The MoP NPs fabricated by two-step reaction coincided with this general trend, showing higher HER activity as the P/Mo ratio increased, while the samples obtained through one-pot reaction did not show high P/Mo dependency.

XPS analysis was conducted to further understand surface chemistry regarding the composition and chemical state of the MoP NPs synthesized via the two different methods for 4 h. The Mo 3d and P 2p spectra of all the samples revealed that the Mo species was chemically well-bonded with the P species. Fig. 5(a) shows Mo had three oxidation states ($Mo^{6+}$, $Mo^{5+}$ and $Mo^{4+}$) in the MoP NPs fabricated in both ways [67,68]. The satellite peak at 231.5-228.4 eV can be ascribed to $Mo^{\delta+}$ species ($0<\delta\leq4$) generally regarded as Mo-P bonding, confirming the successful conversion from Mo metal into MoP [69]. The intensity of the Mo-P peak of the samples prepared via the two-step method was higher compared to the high-oxidation doublet peaks at 236.7-233.4 eV ($Mo^{6+}$) and 234.5-231.3 eV ($Mo^{5+}$); in contrast, it was lower than the intensities of the peaks at 236.7-233.4 eV ($Mo^{6+}$) for the one-pot synthesized MoP NPs. These Mo XPS results suggest that the MoP NPs obtained through the two-step reaction showing high catalytic activity had relatively abundant Mo-P bonds and less-oxidation species on the surface, well matching the previous report that less oxidized Mo metal induced the highest catalytic activity [70].

The peak of the one-pot and two-step prepared MoP (134.7 and 134.5 eV, respectively) can be assigned to the phosphate species formed by surface oxidation [71]. The doublets (130.5-129.5 eV for the two-step method and 130.4-129.6 eV for the one-pot approach) at a similar binding energy position are representative of Mo-P species, further confirming the insertion of P into the Mo structure. The XPS spectra of the samples synthesized via the two methods showed different intensities, reflecting the relative amounts of oxidized species and bonds between Mo and P. The highest intrinsic electrocatalytic activity of the MoP NPs synthesized through the two-step method might be attributed to synergetic effect of various factors combining the presence of numerous Mo-P bonds, the relatively less-oxidized Mo and P species, high P/Mo ratio, and high surface area.

## CONCLUSION

We demonstrated that the type of synthetic method and the conditions adopted to prepare colloidal MoP NPs influence their catalytic performance; moreover, the difference in the catalytic activity is more evident for longer reaction times. Despite the similar size and shape, the MoP NPs prepared via the two methods showed significantly different electrochemical activity. Those synthesized through the two-step approach for 4 h showed the highest intrinsic catalytic activity, requiring an overpotential of 177 mV at a current density of 10 mA $cm^{-2}$, which was lower than that of the sample prepared via the one-pot method with the same reaction time. The EIS results showed the lowest charge transfer resistance with a small-area semicircle of the two-step synthesized MoP NPs (reaction time of 4 h). The XPS analysis revealed that the samples prepared through the two-step reaction form more chemical bonds between metal and phosphorus and less-oxidized Mo species, leading to higher electrocatalytic activity. This comparison of catalytic activity and morphology between different colloidal synthetic methods and reaction times provides new insights about the selection of the synthetic route and might be the key to

boosting the electrocatalytic activity of metal phosphide NPs.

## ACKNOWLEDGEMENTS

This research was supported by Basic Science Research Program through the National Research Foundation of Korea (NRF) funded by the Ministry of Education (NRF- 2019R1C1C1010137). This research was also supported by Hydrogen Energy Innovation Technology Development Program through the National Research Foundation of Korea (NRF) funded by Ministry of Science and ICT (NRF-2019M3E6A1063676).

## CONFLICT OF INTEREST

The authors declare no conflict of interest.

## SUPPORTING INFORMATION

Additional information as noted in the text. This information is available via the Internet at http://www.springer.com/chemistry/journal/11814.

## REFERENCES

1. W. Lubitz and W. Tumas, *Chem. Rev.*, **107**, 3900 (2007).
2. J. A. Turner, *Science*, **305**, 972 (2004).
3. N. S. Lewis and D. G. Nocera, *Proc. Natl. Acad. Sci. USA*, **103**, 15729 (2006).
4. P. Du and R. Eisenberg, *Energy Environ. Sci.*, **5**, 6012 (2012).
5. T. Bak, J. Nowotny, M. Rekas and C. C. Sorrell, *Int. J. Hydrogen Energy*, **27**, 991 (2002).
6. J. D. Benck, Z. Chen, L. Y. Kuritzky, A. J. Forman and T. F. Jaramillo, *ACS Catal.*, **2**, 1916 (2012).
7. M. G. Walter, E. L. Warren, J. R. McKone, S. W. Boettcher, Q. Mi, E. A. Santori and N. S. Lewis, *Chem. Rev.*, **110**, 6446 (2010).
8. Y. Hara, N. Minami, H. Matsumoto and H. Itagaki, *Appl. Catal. A*, **332**, 289 (2007).
9. H. B. Gray, *Nat. Chem.*, **1**, 7 (2009).
10. J. F. Callejas, J. M. McEnaney, C. G. Read, J. C. Crompton, A. J. Biacchi, E. J. Popczun and R. E. Schaak, *ACS Nano*, **8**, 11101 (2014).
11. S. Meyer, A. V. Nikiforov, I. M. Petrushina, K. Köhler, E. Christensen, J. O. Jensen and N. J. Bjerrum, *Int. J. Hydrogen Energy*, **40**, 2905 (2015).
12. W.-F. Chen, J. T. Muckerman and E. Fujita, *Chem. Commun.*, **49**, 8896 (2013).
13. Q. Liu, J. Tian, W. Cui, P. Jiang, N. Cheng, A. M. Asiri and X. Sun, *Angew. Chem. Int. Ed.*, **53**, 6710 (2014).
14. E. J. Popczun, J. R. McKone, C. G. Read, A. J. Biacchi, A. M. Wiltrout, N. S. Lewis and R. E. Schaak, *J. Am. Chem. Soc.*, **135**, 9267 (2013).
15. J. Kibsgaard, C. Tsai, K. Chan, J. D. Benck, J. K. Nørskov, F. Abild-Pedersen and T. F. Jaramillo, *Energy Environ. Sci.*, **8**, 3022 (2015).
16. D. Kong, J. J. Cha, H. Wang, H. R. Lee and Y. Cui, *Energy Environ. Sci.*, **6**, 3553 (2013).
17. C. Tsai, K. Chan, J. K. Nørskov and F. Abild-Pedersen, *Surf. Sci.*, **640**, 133 (2015).
18. J. Bonde, P. G. Moses, T. F. Jaramillo, J. K. Nørskov and I. Chorkendorff, *Faraday Discuss.*, **140**, 219 (2009).
19. Y. Guo, T. Park, J. W. Yi, J. Henzie, J. Kim, Z. Wang and Y. Yamauchi, *Adv. Mater.*, **31**, 1807134 (2019).
20. Z. Huang, Z. Chen, Z. Chen, C. Lv, M. G. Humphrey and C. Zhang, *Nano Energy*, **9**, 373 (2014).
21. J. Kibsgaard and T. F. Jaramillo, *Angew. Chem. Int. Ed.*, **53**, 14433 (2014).
22. E. J. Popczun, C. G. Read, C. W. Roske, N. S. Lewis and R. E. Schaak, *Angew. Chem. Int. Ed.*, **53**, 5427 (2014).
23. P. Xiao, W. Chen and X. Wang, *Adv. Energy Mater.*, **5**, 1500985 (2015).
24. Y. Shi and B. Zhang, *Chem. Soc. Rev.*, **45**, 1529 (2016).
25. D.-H. Ha, B. Han, M. Risch, L. Giordano, K. P. C. Yao, P. Karayaylali and Y. Shao-Horn, *Nano Energy*, **29**, 37 (2016).
26. J. F. Callejas, C. G. Read, E. J. Popczun, J. M. McEnaney and R. E. Schaak, *Chem. Mater.*, **27**, 3769 (2015).
27. C. Y. Son, I. H. Kwak, Y. R. Lim and J. Park, *Chem. Commun.*, **52**, 2819 (2016).
28. D. E. Schipper, Z. Zhao, H. Thirumalai, A. P. Leitner, S. L. Donaldson, A. Kumar and K. H. Whitmire, *Chem. Mater.*, **30**, 3588 (2018).
29. L. Feng, H. Vrubel, M. Bensimon and X. Hu, *Phys. Chem. Chem. Phys.*, **16**, 5917 (2014).
30. L.-A. Stern, L. Feng, F. Song and X. Hu, *Energy Environ. Sci.*, **8**, 2347 (2015).
31. J. M. McEnaney, J. C. Crompton, J. F. Callejas, E. J. Popczun, C. G. Read, N. S. Lewis and R. E. Schaak, *Chem. Commun.*, **50**, 11026 (2014).
32. Z. Xing, Q. Liu, A. M. Asiri and X. Sun, *Adv. Mater.*, **26**, 5702 (2014).
33. J. M. McEnaney, J. C. Crompton, J. F. Callejas, E. J. Popczun, A. J. Biacchi, N. S. Lewis and R. E. Schaak, *Chem. Mater.*, **26**, 4826 (2014).
34. W. Xiao, L. Zhang, D. Bukhvalov, Z. Chen, Z. Zou, L. Shang and T. Zhang, *Nano Energy*, **70**, 104445 (2020).
35. H. Yan, Y. Jiao, A. Wu, C. Tian, X. Zhang, L. Wang and H. Fu, *Chem. Commun.*, **52**, 9530 (2016).
36. H. Vrubel and X. Hu, *Angew. Chem. Int. Ed.*, **51**, 12703 (2012).
37. H. Park, A. Encinas, J. P. Scheifers, Y. Zhang and B. P. T. Fokwa, *Angew. Chem. Int. Ed.*, **56**, 5575 (2017).
38. Y. Jin, H. Wang, J. Li, X. Yue, Y. Han, P. K. Shen and Y. Cui, *Adv. Mater.*, **28**, 3785 (2016).
39. Z. Lu, H. Zhang, W. Zhu, X. Yu, Y. Kuang, Z. Chang and X. Sun, *Chem. Commun.*, **49**, 7516 (2013).
40. D. Wang, Z. Pan, Z. Wu, Z. Wang and Z. Liu, *J. Power Sources*, **264**, 229 (2014).
41. O. Mitsutaka, T. Susumu, I. Masakazu and H. Masatake, *Chem. Lett.*, **27**, 315 (1998).
42. W. Li, S. Ismat Shah, C. P. Huang, O. Jung and C. Ni, *Mater. Sci. Eng. B*, **96**, 247 (2002).
43. S. T. Christensen, H. Feng, J. L. Libera, N. Guo, J. T. Miller, P. C. Stair and J. W. Elam, *Nano Lett.*, **10**, 3047 (2010).
44. S. T. Christensen, J. W. Elam, F. A. Rabuffetti, Q. Ma, S. J. Weigand, B. Lee and M. J. Bedzyk, *Small*, **5**, 750 (2009).
45. S. C. Tsai, Y. L. Song, C. S. Tsai, C. C. Yang, W. Y. Chiu and H. M. Lin, *J. Mater. Sci.*, **39**, 3647 (2004).
46. W. Y. Teoh, R. Amal and L. Mädler, *Nanoscale*, **2**, 1324 (2010).

47. R. A. Khaydarov, R. R. Khaydarov, O. Gapurova, Y. Estrin and T. Scheper, *J. Nanopart. Res.*, **11**, 1193 (2009).
48. Z.-Y. Zhou, N. Tian, Z.-Z. Huang, D.-J. Chen and S.-G. Sun, *Faraday Discuss.*, **140**, 81 (2009).
49. H. Ma, B. Yin, S. Wang, Y. Jiao, W. Pan, S. Huang and F. Meng, *ChemPhysChem.*, **5**, 68 (2004).
50. C. d. M. Donegá, *Chem. Soc. Rev.*, **40**, 1512 (2011).
51. Z. Nie, A. Petukhova and E. Kumacheva, *Nat. Nanotechnol.*, **5**, 15 (2010).
52. D. V. Talapin, J.-S. Lee, M. V. Kovalenko and E. V. Shevchenko, *Chem. Rev.*, **110**, 389 (2010).
53. G. Cho, Y. Park, Y.-K. Hong and D.-H. Ha, *Nano Convergence*, **6**, 17 (2019).
54. E. Lindstedt, M. Reitti and B. Olofsson, *J. Org. Chem.*, **82**, 11909 (2017).
55. H. Dong, M. Zhu, J. A. Yoon, H. Gao, R. Jin and K. Matyjaszewski, *J. Am. Chem. Soc.*, **30**, 12852 (2008).
56. F. Hussain, S. M. Shaban, J. Kim and D.-H. Kim, *Korean J. Chem. Eng.*, **36**, 988 (2019).
57. J. Park, J. Joo, S. G. Kwon, Y. Jang and T. Hyeon, *Angew. Chem. Int. Ed.*, **46**, 4630 (2007).
58. E. Muthuswamy, P. R. Kharel, G. Lawes and S. L. Brock, *ACS Nano*, **3**, 2383 (2009).
59. J. Liu, M. Meyns, T. Zhang, J. Arbiol, A. Cabot and A. Shavel, *Chem. Mater.*, **30**, 1799 (2018).
60. V. V. T. Doan-Nguyen, S. Zhang, E. B. Trigg, R. Agarwal, J. Li, D. Su and C. B. Murray, *ACS Nano*, **9**, 8108 (2015).
61. M. D. Tessier, K. De Nolf, D. Dupont, D. Sinnaeve, J. De Roo and Z. Hens, *J. Am. Chem. Soc.*, **138**, 5923 (2016).
62. H. Li, C. Jia, X. Meng and H. Li, *Front. Chem.*, **6**, 6 (2019).
63. G. Cho, Y. Park, H. Kang, Y.-k. Hong, T. Lee and D.-H. Ha, *Appl. Surf. Sci.*, **510**, 145427 (2020).
64. J. Ryu, N. Jung, J. H. Jang, H.-J. Kim and S. J. Yoo, *ACS Catal.*, **5**, 4066 (2015).
65. J. F. Callejas, C. G. Read, E. J. Popczun, J. M. McEnaney and R. E. Schaak, *Chem. Mater.*, **27**, 3769 (2015).
66. A. B. Laursen, K. R. Patraju, M. J. Whitaker, M. Retuerto, T. Sarkar, N. Yao and G. C. Dismukes, *Energy Environ. Sci.*, **8**, 1027 (2015).
67. M. Hou, X. Teng, J. Wang, Y. Liu, L. Guo, L. Ji and Z. Chen, *Nanoscale*, **10**, 14594 (2018).
68. F. Dury and E. M. Gaigneaux, *Catal. Today*, **117**, 46 (2006).
69. J. Kibsgaard and T. F. Jaramillo, *Angew. Chem. Int. Ed.*, **53**, 14433 (2014).
70. C. Deng, F. Ding, X. Li, Y. Guo, W. Ni, H. Yan and Y.-M. Yan, *J. Mater. Chem. A*, **4**, 59 (2016).
71. M. A. R. Anjum and J. S. Lee, *ACS Catal.*, **7**, 3030 (2017).

# Supporting Information

# Colloidal synthetic methods of amorphous molybdenum phosphide nanoparticles for hydrogen evolution reaction catalysts

**Hyeri Kang*,‡, Taegyeom Lee*,‡, Yoonsu Park*, Yun-Kun Hong*, Miri Choi**, Jiung Cho***, and Don-Hyung Ha*,†**

*School of Integrative Engineering, Chung-Ang University, Seoul 06974, Korea
**Chuncheon Center, Korea Basic Science Institute, Chuncheon 24341, Korea
***Western Seoul Center, Korea Basic Science Institute, Seoul 03579, Korea
(*Received 31 March 2020 • Revised 10 May 2020 • Accepted 11 May 2020*)

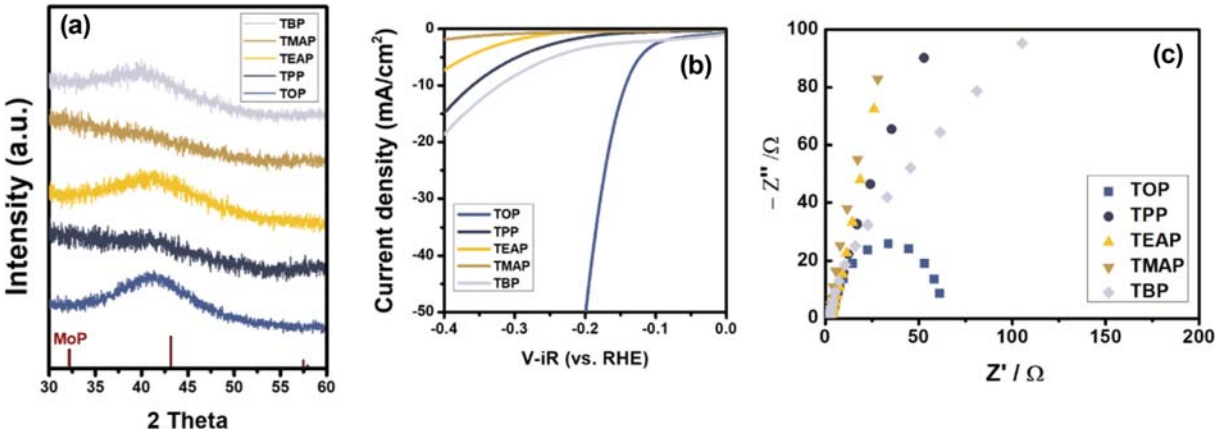


**Fig. S1. (a) XRD patterns of the MoP NP samples synthesized with different phosphorus sources (red bars correspond to Powder Diffraction 03-065-6024). (b) Polarization curves of the MoP NP samples synthesized with different phosphorus sources. (c) Nyquist plots for the MoP NP samples synthesized with different phosphorus sources in 0.5 M $H_2SO_4$ with loading amount of 160 μg $cm^{-2}_{geo}$.**

**Table S1. Electrochemical results of the MoP NP samples synthesized with one-pot reaction for HER in 0.5 M $H_2SO_4$**

One-pot method

| Samples | $\eta$ @10 mA/cm$^2$ | $R_{ct1}$ | $R_{ct2}$ | $C_{dl}$ |
|---|---|---|---|---|
| 30 min | 228 mV | 559.95 Ω | 4.8455 Ω | 1.47 mF/cm$^2$ |
| 2 h | 224 mV | 510.96 Ω | 2.8946 Ω | 1.69 mF/cm$^2$ |
| 4 h | 208 mV | 331.79 Ω | 3.2683 Ω | 1.46 mF/cm$^2$ |

**Table S2. Electrochemical results of the MoP NP samples synthesized with two-step reaction for HER in 0.5 M $H_2SO_4$**

Two-step method

| Samples | $\eta$ @10 mA/cm$^2$ | $R_{ct1}$ | $R_{ct2}$ | $C_{dl}$ |
|---|---|---|---|---|
| 30 min | 196 mV | 338.13 Ω | 3.8673 Ω | 2.8 mF/cm$^2$ |
| 2 h | 190 mV | 318.79 Ω | 4.2481 Ω | 2.78 mF/cm$^2$ |
| 4 h | 177 mV | 180.62 Ω | 1.866 Ω | 2.52 mF/cm$^2$ |

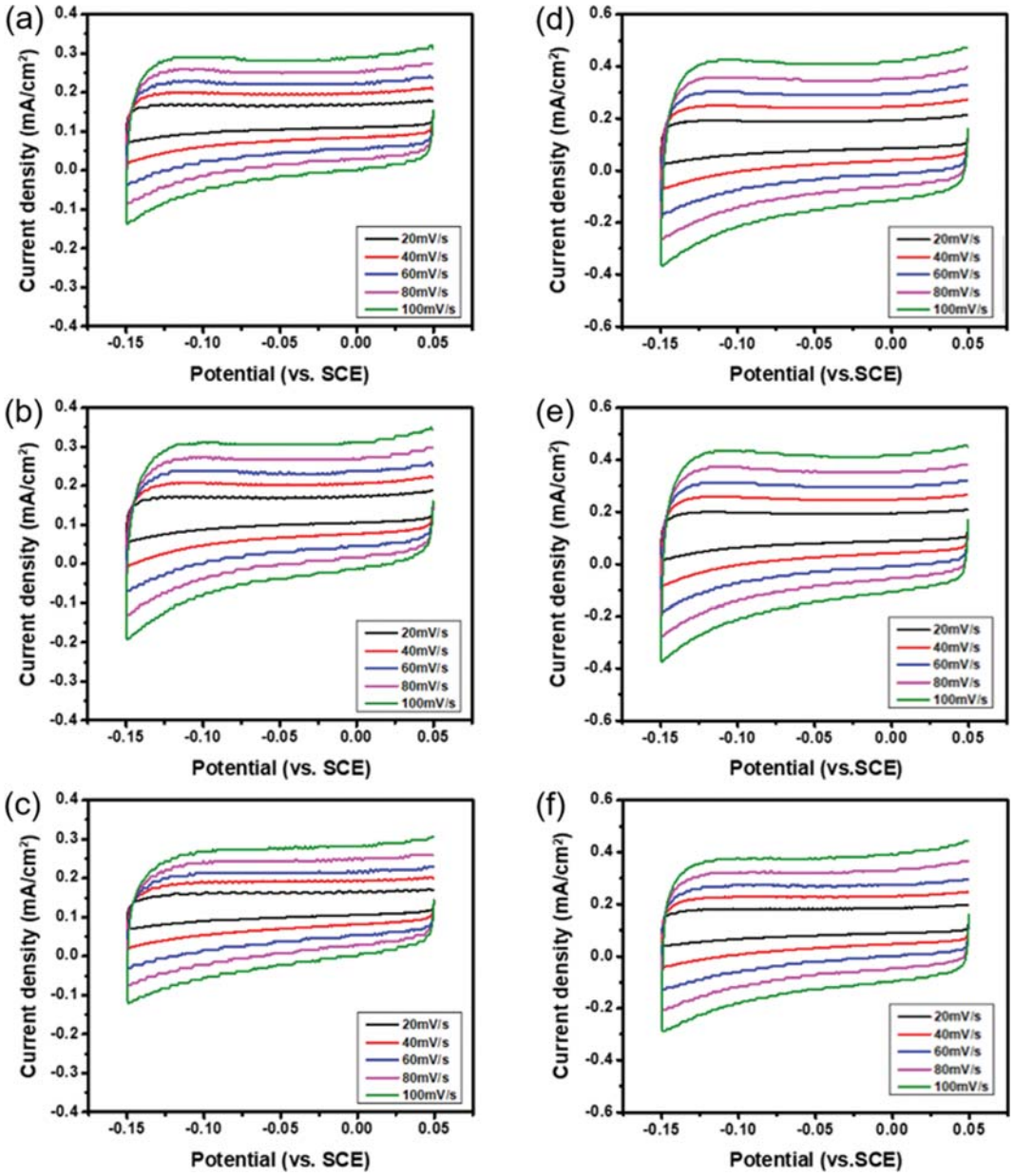


**Fig. S2. CV curves for the MoP NP samples synthesized with (a) one-pot 30 min, (b) one-pot 2 h, (c) one-pot 4 h, (d) two-step 30 min, (e) two-step 2 h and (f) two-step 4 h at various rates from 20 to 100 mV $s^{-1}$.**